

Towards a Low-Cost Wavepacket Model of the Jet Noise Source

Dimitri Papamoschou*, Juntao Xiong[†], and Feng Liu[‡]

University of California, Irvine, Irvine, CA, 92697, USA

We discuss the development of a simplified model for the jet noise source that can be used in practical predictions of installed noise. In the proposed scheme, the source is prescribed on a radiator surface defining the boundary between the inner rotational jet flow and the outer linear pressure field. The source consists of wavepacket-type partial fields whose noise propagation can be computed using well-established linear methods. The complete solution entails synthesizing the partial-field solutions based on the probability density functions of the partial fields. The ability of low-cost Reynolds Averaged Navier Stokes (RANS) solution of the flow field to guide the wavepacket formulation is assessed. The RANS solution is accompanied by acoustic analogy based matching of the far-field spectra to determine the coefficients of the appropriate time and length scales. The RANS-derived velocity, length, and time scales are compared with those obtained using Large Eddy Simulation (LES) of a cold Mach 0.9 jet. The RANS quantities are assessed on the surface of peak turbulent kinetic energy while the LES statistics are computed on the radiator surface. There is good agreement in the convective velocity, however RANS under-predicts the correlation scales on the radiator surface. The LES provides additional physical insights into the noise source and suggests that the partial fields have limited azimuthal extent.

Nomenclature

a_∞	=	ambient speed of sound
A	=	cross sectional area; amplitude
C	=	correlation coefficient
D_j	=	jet exit diameter
H	=	wavenumber-frequency spectrum
k	=	turbulent kinetic energy
L	=	characteristic length scale
M	=	Mach number
M_c	=	convective Mach number
r	=	distance between source and observer
R	=	observer distance in spherical coordinate system; correlation function
\widehat{R}	=	Fourier transform of correlation function
p	=	static pressure
S	=	spectral density of far-field pressure
u, v, w	=	velocities in Cartesian coordinate system
\tilde{u}	=	characteristic velocity scale
U_c	=	convective velocity
U_j	=	jet exit velocity
y	=	radial coordinate
U_c	=	convective velocity
α	=	acoustic wavenumber = ω/a_∞
$\boldsymbol{\alpha}$	=	wavenumber vector in direction of observer = $\alpha\mathbf{x}/R$

*Professor, Department of Mechanical and Aerospace Engineering, Fellow AIAA

[†]Postdoctoral Researcher, Department of Mechanical and Aerospace Engineering, Member AIAA

[‡]Professor, Department of Mechanical and Aerospace Engineering, Fellow AIAA

β	=	shape parameter
Γ	=	azimuthal influence function
ϵ	=	dissipation
θ	=	polar angle relative to jet axis
λ	=	acoustic wavelength
ϕ	=	azimuthal angle
Φ	=	azimuthal correlation angle
ρ	=	density
ω	=	angular frequency
Ω	=	specific dissipation = ϵ/k

I. Introduction

The aerospace industry and government agencies have requirements for low-cost prediction of aircraft engine noise, with turnaround times on the order of hours. Community noise and exposure of military personnel to near-field sound are becoming prominent factors in the design of new commercial and military engines. Prediction of jet turbulent mixing noise and its interaction with airframe surfaces constitutes an immense theoretical and computational challenge. The noise source is stochastic and highly sensitive on the instantaneous and time-averaged features of the jet flow. Common scattering techniques are designed for deterministic, not random fields. A solution from first principles, while possible in principle, would require inordinate computational resources and time for a single solution, thus cannot be considered a practical predictive tool. We seek simplification of the jet noise source that retains the basic physics and, with strategic empiricism, will yield high-fidelity predictions of the radiated sound and its scattering around objects at relatively low computational cost.

A possible predictive scheme is presented at a simplified level in Fig. 1. The essence of the approach is that the jet noise source is represented on a conical-shaped “radiator surface” on the boundary between the inner nonlinear rotational flow field and outer linear pressure field. Once the noise source on the radiator surface is properly modeled, propagation to an observer outside the surface involves well established linear tools, such as the boundary element method (BEM). To model the noise source, we need information on the flow field that is not computationally expensive to obtain. Today the Reynolds Averaged Navier Stokes (RANS) solution of the jet plume constitutes the backbone of acoustic-analogy based noise predictions. These computations are relatively low-cost and, with moderate resources, can be obtained in a matter of hours. The major question is whether the RANS solution can inform the prescription of the noise source on the radiator surface. The current study addresses this topic by comparing relevant statistics computed by RANS and Large Eddy Simulation (LES) of a Mach 0.9 cold jet.

II. Wavepacket Model of Jet Noise

A. Prediction Scheme

The pressure field on the radiator surface will be synthesized from elementary sources, or partial fields, that capture the nature of jet mixing noise. These can be considered as the building blocks for the full solution. Turbulent mixing noise is dominated by large-scale, “coherent” turbulent eddies in the shear layers forming the initial region of the jet and in the region past the end of the potential core. These eddies are of integral length scale, thus defining the extent of the mixing region, and convect downstream with a velocity U_c that is a fraction (typically $\sim 60\%$) of the local centerline mean velocity. Because these structures grow with downstream distance, they merge with each other - a phenomenon often referred to as vortex pairing.¹ The merger process imparts a lifetime to each vortex, which we can connect to an axial coherence length scale. In addition, the eddies have a finite azimuthal coherence scale. Just outside the jet, in the near pressure field, the pressure distribution reflects the “footprint” of the eddies, as confirmed by several studies.^{2,3} Therefore we expect that random events on the radiator surface have similar features as the turbulent eddies whose footprint is sensed on that surface, namely similar coherence scales and convective velocity.

This leads to the “wavepacket” representation of the near pressure field, a characterization of the jet noise source that has been the subject of numerous works and is gaining acceptance as a physical approximation

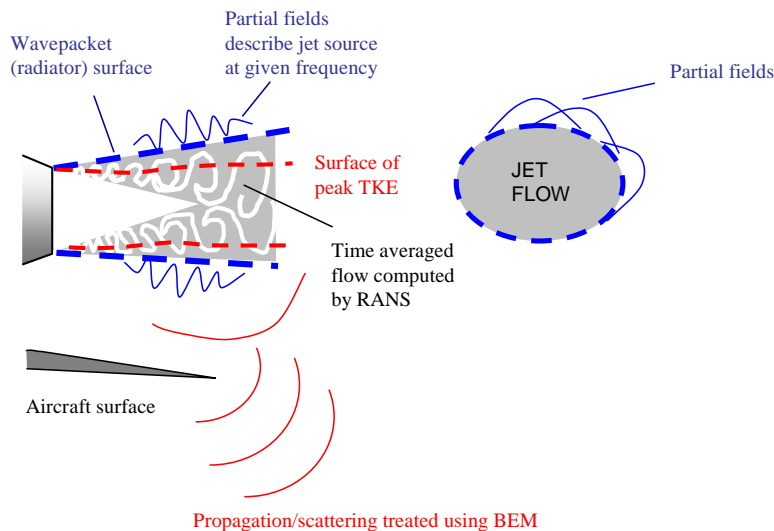


Figure 1. Basic elements of predictive scheme for jet noise and its interactions.

of the source.⁴⁻⁸ A cartoon representation of our formulation of the wavepacket is shown in Fig. 2. It is an amplitude modulated traveling wave, the modulation envelope having finite extents in the axial and azimuthal directions, X and Q , respectively. The limited extent of the wavepacket is supported by measurements of the axial and azimuthal coherence of the near-pressure field⁹⁻¹¹ as well as correlation measurements of the turbulent velocity and temperature fields inside the jet.¹² The wavepacket is further characterized by the convective velocity U_c , the helicity β , and the precise shape of the modulation envelope. The proposed mathematical representation of the wavepacket partial field is inspired by a number of past works.¹³⁻¹⁵ For a given frequency ω , the partial field is

$$p(t, x, \phi) = \epsilon F\left(\frac{x - x'}{X}\right) G\left(\frac{\phi - \phi'}{Q/y_{edge}}\right) \exp\left[i\frac{\omega}{U_c}(x - x' - U_c t) + i\beta(\phi - \phi')\right] \quad (1)$$

Here F and G are deterministic functions defining the axial and azimuthal envelope shapes; y_{edge} is the surface radius at the event location; x' and ϕ' are independent random variables representing the stochastic origin of each event; and ϵ is a random amplitude, independent of x' and ϕ' . For an azimuthally coherent field, the helicity β becomes the helical mode m , which must be an integer; however, if the azimuthal coherence is finite, the helicity can be represented in terms of a non-integer variable. Initial wavepacket models indicate that the helicity of the wavepacket field must increase with frequency.¹³ Equation 1 represents a random event, or partial field, on the radiator surface. A number of such events will be necessary to reconstruct the statistics of the pressure field at a given frequency. In other words, the random source will be represented as an assembly of deterministic partial fields, each field having being parameterized and assigned a probability density function (pdf).

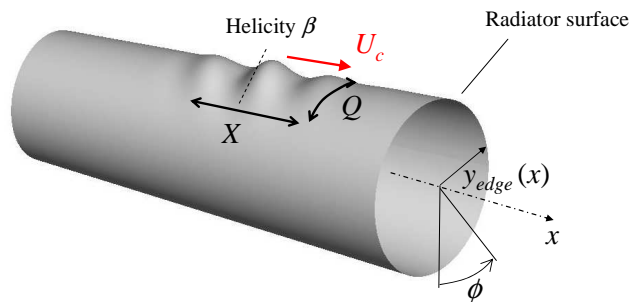


Figure 2. Cartoon representation of a wavepacket event (partial field).

Past wavepacket parameterizations captured the far-field sound pressure level in a free field environment,¹³ and showed promise for predicting the diffraction of jet noise from solid boundaries.¹⁶ In those studies the sound source was essentially deterministic (one or two partial fields was used) and the parameterization was done “blindly”, with some constraints on the convective velocity, without knowledge of the underlying jet flow. A more realistic prediction of jet noise and its scattering needs to incorporate the base flow, at least in a time-averaged sense, and use a number of partial fields. This is where RANS is expected to play a key role by providing the relevant length and velocity scales that will guide the wavepacket parameterization. These scales will serve as constraints in the parameterization process, wherein the parameters are determined by minimizing a cost function. The cost function would be based on the difference between modeled and actual noise statistics, such as the far-field sound pressure level or the near-field cross-spectral matrix.

As expressed in Eq. 1 and illustrated in Fig. 2, the wavepacket spatial extent is defined by the scales X and Q . These are frequency-dependent scales. Because the characteristic frequency is a strong function of axial position x , these scales may also be expressed as $X(x)$ and $Q(x)$. The convective velocity is also a function of x . In a simple single-stream jet, U_c is fairly constant in the shear layer surrounding the potential core, then decays as the centerline velocity drops past the end of the potential core. In multi-stream jets, the determination of U_c is more complex and depends on the interactions between the various shear layers defining the initial region of the jet.¹⁵ Proper modeling of U_c is crucial for capturing the radiation efficiency of these jets.¹⁷

The present study is concerned with modeling the distribution of correlation scales, frequency distribution, and convective velocity on the radiator surface. It should be noted that the spatial correlation scales are not equal to the partial field scales in Eq. 1. Correlation scales are created once the various partial fields are synthesized into statistics on the radiator surface. Thus there are additional elements of the problem, such as the assignment of probability density functions for the random variables in Eq. 1, that need to be worked before a predictive scheme can be implemented. These will be topics for follow-on investigations.

B. Radiator Surface

Any surface surrounding the jet that does not include the vortical field can be used as a “source surface” to propagate outward and compute the sound field. That surface would have a particular distribution of U_c , depending on its shape (e.g., cone, cylinder, etc), and its distance from the jet axis. However, there is only one such surface that contains the full hydrodynamic component of the pressure field, that is, the signature of the turbulent motion of the eddies inside the jet. This surface is the edge of the jet, defined here as the closest surface to the jet centerline on and outside of which the propagation of pressure perturbation is governed by the homogeneous linear wave equation. If a connection is to be made between a fluid-mechanical velocity and a convective velocity in the linear pressure field, the latter would need to be defined on the edge surface. Outside the edge surface, the hydrodynamic information is lost quickly.

We discuss the criterion for determining the boundary between the jet flow and the linear pressure field generated by the jet. We define the linear pressure field as the region surrounding the jet where the propagation of pressure is governed by the homogeneous linear wave equation. To quantify this definition, we examine an axisymmetric flow on the (x, y) plane with unidirectional mean velocity $\bar{\mathbf{u}} = (\bar{u}(y), 0, 0)$ and mean speed of sound $\bar{a}(y)$. We impose small (linear) perturbations $\mathbf{u}' = (u', v')$, ρ' , and p' . The perturbations are thus governed by the linear Euler equations, which under the aforementioned conditions yield the following equation for the pressure:¹⁸

$$\frac{\bar{D}}{Dt} \left[\frac{1}{\bar{a}^2} \frac{\bar{D}^2 p'}{Dt^2} - \nabla^2 p' \right] = -2 \frac{d\bar{u}}{dy} \frac{\partial^2 p'}{\partial x \partial y} \quad (2)$$

where $\bar{D}/Dt \equiv \partial/\partial t + \bar{u}\partial/\partial x$. When the right hand vanishes, the pressure is governed by the homogeneous convective wave equation and thus our criterion is satisfied. Order of magnitude analysis yields

$$\frac{a}{\lambda^3} [p'] = \frac{d\bar{u}}{dy} \frac{1}{\lambda^2} [p'] \quad (3)$$

where λ is the acoustic wavelength. Letting $f_c = a/\lambda$ denote the characteristic frequency of noise emission, the above is rewritten as

$$[p'] = \frac{1}{f_c} \frac{d\bar{u}}{dy} [p'] \quad (4)$$

Hence the criterion for the linear pressure field is

$$\frac{1}{f_c} \frac{d\bar{u}}{dy} \rightarrow 0 \quad (5)$$

Extending this relation to a slowly developing jet flow, the characteristic frequency is connected to the integral thickness $\delta(x)$ and the mean centerline jet velocity $u_0(x)$ via

$$f_c = \frac{u_0(x)}{\delta(x)} \quad (6)$$

Selecting δ as the vorticity thickness,

$$\delta = \frac{u_0}{(d\bar{u}/dy)_{max}} \quad (7)$$

the characteristic frequency is

$$f_c = (d\bar{u}/dy)_{max} \quad (8)$$

and thus the criterion becomes

$$\frac{d\bar{u}/dy}{(d\bar{u}/dy)_{max}} \rightarrow 0 \quad (9)$$

Accordingly, the edge $y_{edge}(x)$ is defined as the radial position where the radial gradient of the mean axial velocity, normalized by its local peak value, equals a given threshold $\kappa \ll 1$:

$$\frac{|d\bar{u}/dy|(x, y_{edge}(x))}{|d\bar{u}/dy|_{max}(x)} = \kappa \quad (10)$$

The threshold selected here is $\kappa = 0.01$.

III. RANS-Derived Scales

The basic steps for determining the length and velocity scales from the RANS flow field are:

- Computation of the RANS flow field. This yields the mean velocity, turbulent kinetic energy (k), and specific dissipation (Ω) fields. Coherence length and time (or frequency) scales are constructed based on dimensional combinations of k and Ω . These constructions involve non-dimensional coefficients to be estimated in the next step.
- Far-field acoustic analogy modeling based on the RANS flow field, wherein the problem is parameterized in terms of the scale coefficients and shapes of the correlation functions. The approach in Ref. 15 is followed, where the parameters are estimated by minimizing the difference between the modeled and experimental far-field sound pressure level. This process generates the desired scale coefficients.
- Determination of the coherence scales and convective velocity on the surface of peak turbulent kinetic energy (k_{max} in the RANS flow field (red dashed line in Fig. 1). The most energetic turbulence (representing the most energetic eddies in the time-resolved flow) occurs on this surface; the footprint of the eddies on the radiator surface is expected to be influenced by the events on the k_{max} surface.

A. RANS Solver

The computational fluid dynamics code used here is known as PARCAE¹⁹ and solves the unsteady three-dimensional Navier-Stokes equations on structured multiblock grids using a cell-centered finite-volume method. Information exchange for flow computation on multiblock grids using multiple CPUs is implemented through the MPI (Message Passing Interface) protocol. In its time-averaged implementation, the code solves the RANS equations using the JST scheme²⁰ and the Shear Stress Transport (SST) turbulence model of Menter.²¹ The SST model combines the advantages of the k - Ω and k - ϵ turbulence models for both wall-bounded and free-stream flows. In its unsteady implementation, the solver uses implicit backward three-layer second-order time integration with explicit five stage Runge-Kutta dual time stepping. The time-evolving jet flow is simulated using a hybrid RANS/LES approach.²² The spatial discretization of the inviscid flux is based on the weighted averaged flux-difference splitting algorithm of Roe.^{23, 24} The viscous flux is discretized using a second-order central difference scheme. Near the wall region the Spalart-Allmaras turbulence model²⁵ is used to model the turbulent viscosity, while in the free shear flow the computation relies on the subtle dissipation of the upwind scheme, using the method proposed by Shur *et al.*²⁴

B. Acoustic Analogy Model

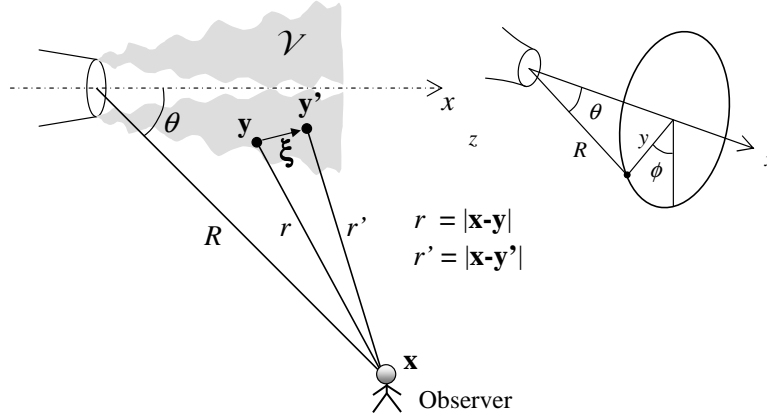


Figure 3. Nomenclature and coordinate system for acoustic analogy model.

We cover only the salient aspects of the theory, with details available in a variety of publications including Refs. 15 and 26. Referring to Fig. 3, the noise source region has volume \mathcal{V} , location \mathbf{y} refers to a point inside the source region, location \mathbf{x} is the observer location outside the source region, $r = |\mathbf{x} - \mathbf{y}|$ is the distance between source and observer, and $\boldsymbol{\xi} = \mathbf{y}' - \mathbf{y}$ denotes the separation vector between two source elements. In the far field, $r \approx R$ and the wavenumber vector $\boldsymbol{\alpha} = \alpha \mathbf{x}/R$ describes the propagation of sound towards the observer. The spectral density of pressure in the far field takes the form

$$S(\mathbf{x}, \omega) = \alpha^4 \int_{\mathcal{V}} |G(\mathbf{x}, \mathbf{y}, \omega)|^2 H(\mathbf{y}, \boldsymbol{\alpha}, \omega) d^3 \mathbf{y} \quad (11)$$

with

$$H(\mathbf{y}, \boldsymbol{\alpha}, \omega) = \int_{\mathcal{V}_{\xi}} \int_{-\infty}^{\infty} R_{xxxx}(\mathbf{y}, \boldsymbol{\xi}, \tau) \exp[i(\boldsymbol{\alpha} \cdot \boldsymbol{\xi} - \omega \tau)] d\tau d^3 \boldsymbol{\xi} \quad (12)$$

Here $G(\mathbf{x}, \mathbf{y}, \omega)$ is a Greens function that describes the propagation of the sound from the source to the observer; $H(\mathbf{y}, \boldsymbol{\alpha}, \omega)$ is the wavenumber frequency spectrum of the equivalent noise sources in the acoustic analogy; and R_{xxxx} is the space-time correlation of the Lighthill stress tensor in the direction of the observer. Equation 12 is a four-dimensional Fourier transform of the space-time correlation over time and over the correlation volume \mathcal{V}_{ξ} . A general form for the space-time correlation is

$$R_{xxxx}(\mathbf{y}, \boldsymbol{\xi}, \tau) = A_{xxxx}(\mathbf{y}) R_1 \left(\frac{\xi_x}{L_{\tau}(\mathbf{y})} \right) R_2 \left(\frac{\xi_y}{L_y(\mathbf{y})} \right) R_3 \left(\frac{\xi_{\phi}}{L_{\phi}(\mathbf{y})} \right) R_4 \left(\frac{\xi_x - \tilde{u}\tau}{L_x(\mathbf{y})} \right) \quad (13)$$

$A_{xxxx}(\mathbf{y})$ is the amplitude of the correlation and has units of $\rho^2 u^4$; $R_1 \dots R_4$ are correlation functions; L_x , L_y , and L_{ϕ} are correlations length scales in the axial, radial and circumferential (azimuthal) directions, respectively; L_{τ} is a length scale that depends on the turbulent time scale τ_* ; and \tilde{u} is a characteristic velocity associated with the convection of the mean flow or the convection of the turbulent eddies. Expecting the contribution of ‘‘shear noise’’ to dominate the direction of peak emission, we set $A_{xxxx} = B \bar{\rho}^2 \tilde{u}^2 k$, where B is a fitting constant. Assuming that the correlations do not have azimuthal variation, the four-dimensional Fourier transform of Eq. 12 yields:

$$H(\mathbf{y}, \boldsymbol{\alpha}, \omega) = B \bar{\rho}^2 \tilde{u}^2 k L_{\tau} L_y L_{\phi} \frac{L_x}{\tilde{u}} \hat{R}_1 \left(\alpha L_{\tau} \frac{\tilde{u} \cos \theta - a_{\infty}}{\tilde{u}} \right) \hat{R}_2(\alpha L_y \sin \theta) \hat{R}_3(0) \hat{R}_4 \left(\frac{\omega L_x}{\tilde{u}} \right) \quad (14)$$

We may select \tilde{u} to be the mean flow velocity or the convection velocity of the turbulent eddies. The two velocities can be very different. In this study we set $\tilde{u} = U_c$ where U_c is the convection velocity of the large-scale structures, consistent with the focus of our work on modeling noise in the direction of peak emission. Then the convective Mach number $M_c = \tilde{u}/a_{\infty} = U_c/a_{\infty}$ represents the Mach number of large-scale structures (instability waves) with respect to the ambient medium. On selecting $L_{\tau} = U_c \tau_*$, Eq. 14

becomes

$$H(\mathbf{y}, \boldsymbol{\alpha}, \omega) = B \bar{\rho}^2 \bar{u}^2 k \tau_* L_x L_y L_\phi \widehat{R}_1(\omega \tau_*(M_c \cos \theta - 1)) \widehat{R}_2(\alpha L_y \sin \theta) \widehat{R}_3(0) \widehat{R}_4\left(\frac{\alpha L_x}{M_c}\right) \quad (15)$$

In recent work¹⁵ the acoustic analogy model was parameterized in terms of the shapes of the correlation functions and the coefficients of the correlation scales. The generic correlation function was selected as

$$R_j(t) = e^{-|t|^{\beta_j}} \quad (16)$$

The correlation length and time scales followed the usual constructions based on the turbulent kinetic energy k and specific dissipation $\Omega = k/\epsilon$ of the RANS-computed flow:

$$\begin{aligned} L_x &= C_1 \frac{k^{1/2}}{\Omega} \\ L_y &= C_2 \frac{k^{1/2}}{\Omega} \\ L_\phi &= C_3 \frac{k^{1/2}}{\Omega} \\ \tau_* &= C_4 \frac{1}{\Omega} \end{aligned} \quad (17)$$

At a given radial position y , the azimuthal angular scale is defined as $\Phi = L_\phi/y$. Assuming equality of radial and circumferential correlations (i.e., $\beta_3 = \beta_2$, $C_3 = C_2$) the far-field spectral density becomes a function of the parameter vector $V = [C_1, C_2, C_4, \beta_1, \beta_2, \beta_4]$. The parameter vector is determined by matching, in a least-squares sense, the experimental spectral density for a baseline jet in a particular polar direction.

For an axisymmetric jet, the Green's function G in Eq. 11 takes the free-field form

$$G = \frac{1}{4\pi R} e^{-i\alpha R} \quad (18)$$

For asymmetric jets, the Green's function needs to account for propagation through the mean flow, a task that formally requires solution of the linear Euler equations. However, considerable simplification is possible by neglecting propagation through the mean flow and applying outward linear propagation from the radiator surface. The wavepacket model describes how a localized azimuthal disturbance spreads with radial distance and polar angle, which allows construction of an azimuthal influence function Γ for the intensity field. An approximate Green's function is then defined as of the form

$$G = \frac{1}{4\pi R} e^{-i\alpha R} \Gamma(\phi(\mathbf{x}) - \phi(\mathbf{y}), \theta(\mathbf{x}), \alpha) \quad (19)$$

where $\phi(\mathbf{y})$ is the azimuthal angle of a given source volume element; and $\theta(\mathbf{x})$ and $\phi(\mathbf{x})$ are the polar and azimuthal coordinates of the far-field observer, respectively. Details of this approach are available in Ref. 15.

C. Determination of Model Parameters

The modeled spectral density in Eq. 11 can be expressed as

$$S(V_k(\theta), \mathbf{x}, \omega)$$

where V_k is the parameter vector discussed in Section III.B. We seek to determine V_k by matching, in a least squares sense, the experimental far-field spectra. It is convenient to work with the Sound Pressure Level (SPL) spectrum, in units of decibels. The modeled SPL spectrum is

$$\text{SPL}_{\text{mod}}(V_k(\theta(\mathbf{x})), \mathbf{x}, \omega) = 10 \log_{10} \left[\frac{S(V_k(\theta(\mathbf{x})), \mathbf{x}, \omega)}{S_{\text{ref}}} \right] \quad (20)$$

with $S_{\text{ref}} = 4 \times 10^{-10} \text{ Pa}^2$. The experimental SPL spectrum is $\text{SPL}_{\text{exp}}(\mathbf{x}, \omega)$. We facilitate the optimization by normalizing the spectrum by its maximum value. Equivalently, in decibels we subtract the maximum

value. The normalization removes the effect of distance R , so the normalized spectrum depends only on the parameter vector and the observer polar angle (recall that the baseline jet is axisymmetric, so there is no azimuthal variation of the spectrum). The normalized modeled and experimental SPL spectra are:

$$\begin{aligned} \text{SPL}_{\text{mod}}^*(V_k(\theta), \omega) &= \text{SPL}_{\text{mod}}(V_k(\theta), R, \omega) - \text{SPL}_{\text{mod, max}}(V_k(\theta), R) \\ \text{SPL}_{\text{exp}}^*(\theta, \omega) &= \text{SPL}_{\text{exp}}(\theta, R, \omega) - \text{SPL}_{\text{exp, max}}(\theta, R) \end{aligned} \quad (21)$$

This normalization removes the amplitude as a variable, so we are concerned only with matching the shape of the spectra.

For a given jet flow, the experimental SPL is known at discrete frequencies ω_j , $j = 1, \dots, J$. We construct a cost function based on the variance between the modeled and experimental SPL at a specific polar angle θ .

$$F(V_k) = \frac{1}{J} \sum_{j=1}^J [\text{SPL}_{\text{mod}}^*(V_k, \omega_j) - \text{SPL}_{\text{exp}}^*(\omega_j)]^2 \quad (22)$$

We then seek determination of V_k that minimizes the cost function. The minimization process of Eq. 22 uses the Restarted Conjugate Gradient method of Shanno and Phua²⁷ (ACM TOM Algorithm 500).

D. Peak TKE Surface

The locus of peak k is a surface around the jet axis defined by the radial location $y_m(x, \phi)$ where k is maximized at given axial location x and azimuthal angle ϕ . The RANS-derived convective velocity is modeled as the mean velocity on this surface:

$$U_c(x, \phi) = \bar{u}(x, y_m(x, \phi), \phi) \quad (23)$$

In the acoustic analogy formulation of the previous section, all the volume elements at a particular x and ϕ are assigned the same value of U_c as defined above. A similar definition for U_c was used by Karabasov *et al.*²⁸ where the convection velocity was determined from the location of the maximum in the fourth-order velocity cross-correlation. For an axisymmetric jet there is no azimuthal dependence, thus $U_c = U_c(x)$.

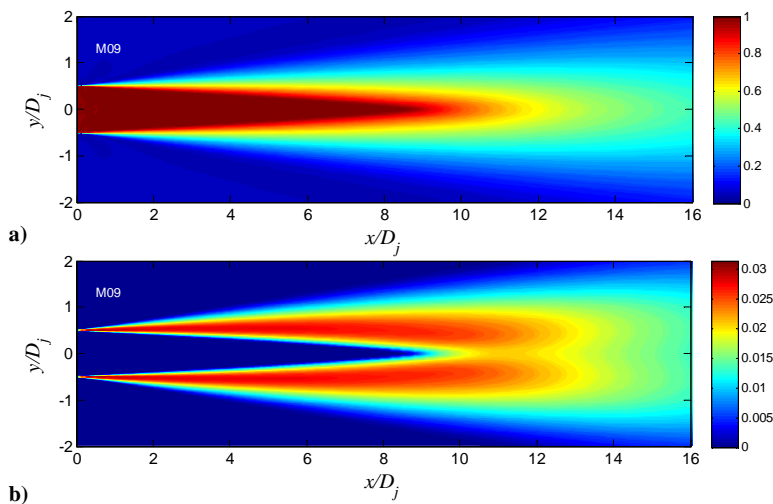


Figure 4. RANS flow field of Mach 0.9 jet. a) Mean axial velocity \bar{u}/U_j ; b) turbulent kinetic energy k/U_j^2 .

E. Results for Mach 0.9 Jet

We consider a single-stream jet with exit diameter $D_j = 0.0218$ m. The jet is supplied by room-temperature air and exhausts at $M_j = 0.9$ and $U_j = 286$ m/s. The acoustic Mach number is $U_j/a_\infty = 0.83$ and the Reynolds number is 300,000 based on exit diameter. The same jet was tested in our aeroacoustics facility where the far-field sound pressure level spectra were measured.

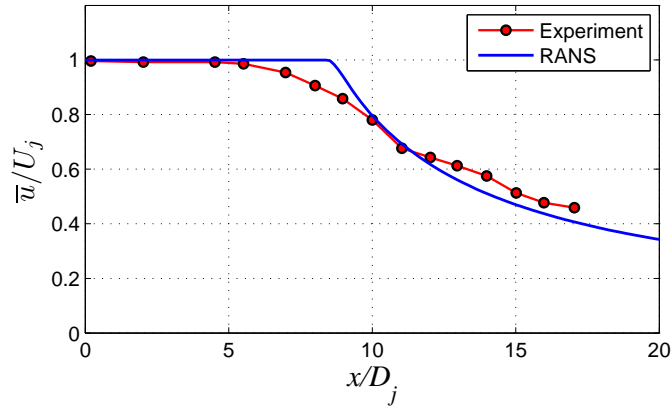


Figure 5. Distribution of RANS-computed centerline mean axial velocity, with comparison to the experimental data of Lau *et al.*²⁹

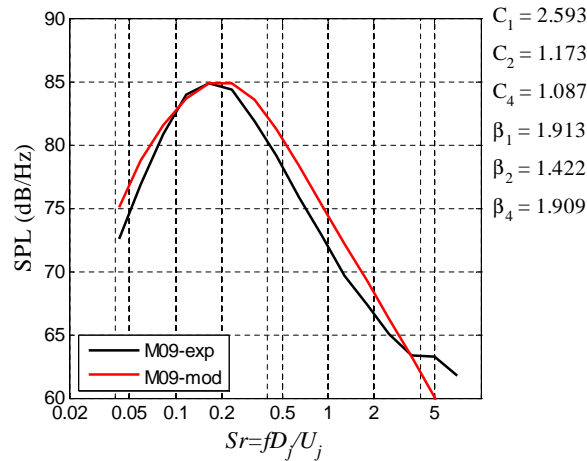


Figure 6. Acoustic analogy parameterization in the direction of peak emission ($\theta = 30^\circ$) for a Mach 0.9 cold jet. Black line: experimental spectrum; red line: modeled spectrum. Model parameters are displayed on right.

For the RANS simulation of dual-stream jets, the computational grid extended $20D_j$ radially from the nozzle centerline and over $60D_j$ downstream of the nozzle. The computational domain had 3.5 million grid points. Fig. 4 shows contour plots of the mean axial velocity and turbulent kinetic energy. Figure 5 plots the centerline mean axial velocity and compares with the experimental data of Lau *et al.*²⁹ The RANS solution over-predicts the length of the potential core by about 20%.

The result of the acoustic analogy parameterization for $\theta = 30^\circ$ (direction of peak emission) is shown in Fig. 6. A good match between the experimental and modeled spectra is noted. The figure displays the resulting parameter vector.

IV. LES-Derived Scales

The same Mach 0.9 jet used in the RANS solution is now treated using Large Eddy Simulation. The purpose of LES is to provide a high-fidelity, time-resolved simulation of the flow field and the pressure field. We will then compare the RANS and LES statistics.

A. Computational Details

The PARCAE code reviewed in Section III.A was used to compute the unsteady flow. The computational grid extended to about $20D_j$ in the radial direction and $60D_j$ in the axial direction. The spatial grid had about 7 million points and 2666 points in time were used with $\Delta t = 6 \mu s$. For the nozzle flow, the total pressure, total temperature, and zero flow angle were specified at the inlet surface corresponding to a perfectly expanded exit Mach number. For the ambient region surrounding the nozzle flow, a non-reflecting characteristic boundary condition was imposed, and a buffer layer was implemented near the outflow. The adiabatic no-slip boundary condition was specified on the nozzle wall. Auto- and cross-spectral densities were computed using a 512-point Fast Fourier Transform and overlapping data blocks. The far-field noise was computed by surface integral with Ffowcs Williams-Hawkings (FWH) formulation without external quadrupoles. The far field pressure is then expressed as the sum of monopole and dipole noise sources.²⁴

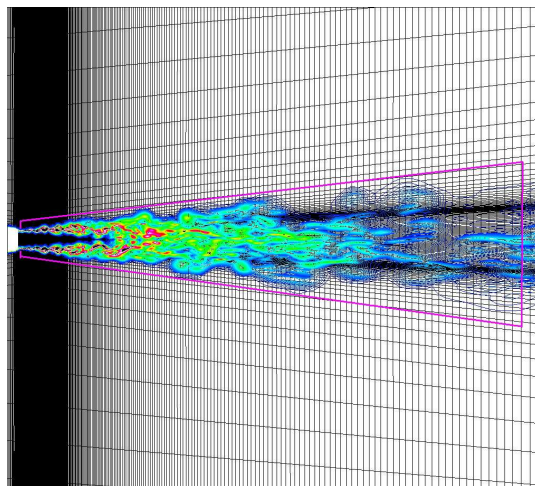


Figure 7. LES computation of Mach 0.9 cold jet: instantaneous vorticity field, computational grid, and FWH surface.

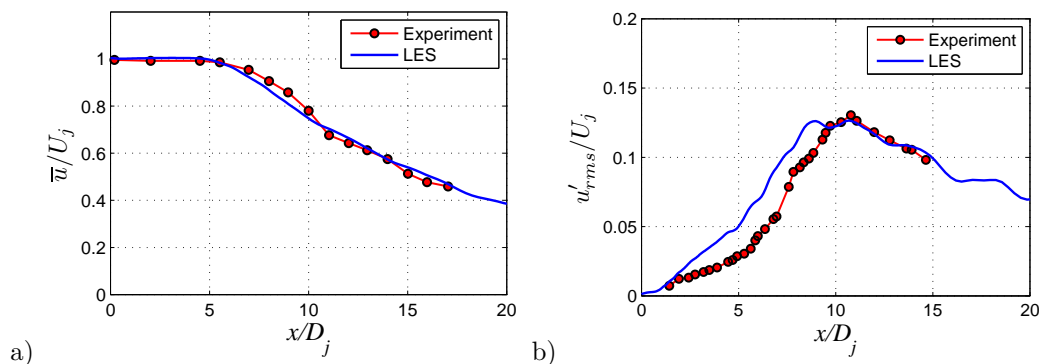


Figure 8. Centerline distributions in LES-computed Mach 0.9 jet, with comparison to the experiments of Lau *et al.*²⁹ a) Mean axial velocity; b) rms axial velocity.

Figure 7 depicts a snapshot of the instantaneous vorticity field, the computational grid used, and the geometry of the Ffowcs Williams - Hawkings (FWH) surface used for computing the radiated sound. The FWH surface extended to $28D_j$. Figure 8 plots the axial distributions of mean and rms axial velocity along the jet centerline. The agreement with the experiments of Lau *et al.*²⁹ is very good. The predictions of the far-field sound pressure levels are compared with experimental measurements in Fig. 9. The agreement is reasonable in the Strouhal number range $[0.1, 2.0]$. These results indicate that the LES is producing physically meaningful data.

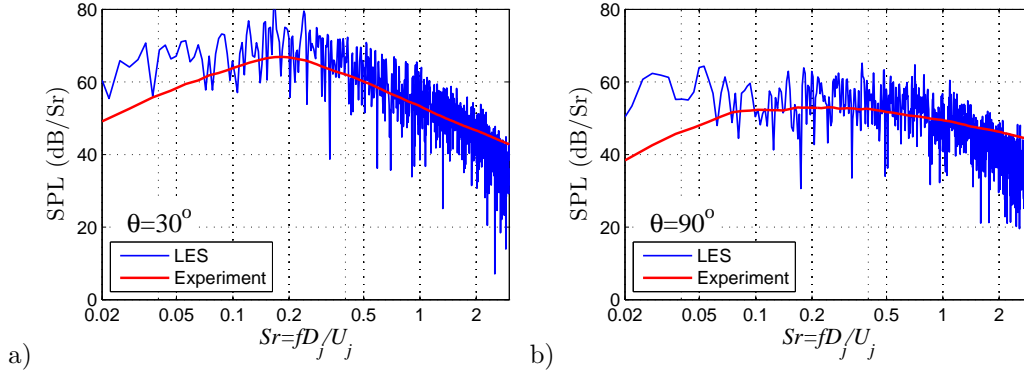


Figure 9. Far-field sound pressure level spectra ($r/D_j=100$) of LES-computed Mach 0.9 jet, with comparisons to experimental measurements at UCI. a) $\theta = 30^\circ$; b) $\theta = 90^\circ$.

B. Axial Space-Time Correlations

The LES solution allows calculation of the space-time correlation anywhere inside and outside the jet flow within the computational domain. Stationarity in time is assumed. We examine the axial space-time correlation of pressure, in the normalized form

$$R_{pp}(x, y; \xi_x, \tau) = \frac{\langle p'(x, y, \phi, t) p'(x + \xi_x, y, \phi, t + \tau) \rangle}{p'_{rms}(x, y) p'_{rms}(x + \xi_x, y)} \quad (24)$$

where $\langle \rangle$ denotes the time average. The correlation for u' produced practically identical results. Example space-time correlations are plotted in Fig. 10.

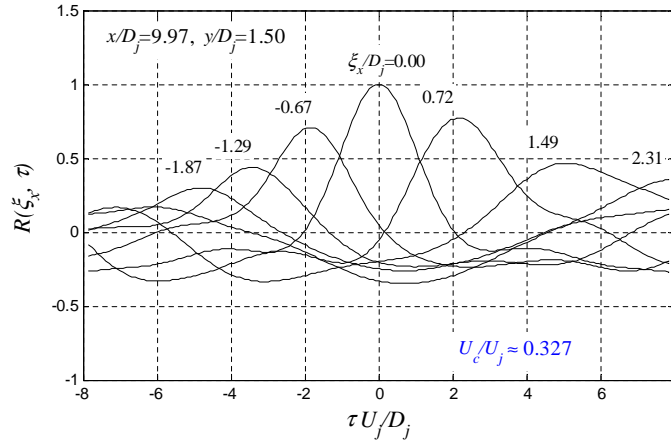


Figure 10. Space-time correlation of pressure at $x/D_j = 10, y/D_j = 1.5$.

Computation of the convective velocity at point (x_m, y_n) of the computational grid involved the space-time correlations at very small axial separations around this point, $\xi_{x,i} = x_{m+i} - x_m$, $i = -2, -1, 1, 2$, where x_k is the axial vector of the computational domain. Small separations were used because the statistics are not stationary in space. Because each correlation function comprises a discrete set of points, to accurately locate the maximum value of the correlation a seventh-order polynomial was fitted around the peak of the correlation curve. The time separation corresponding to the maximum value of the polynomial (i.e., the root of the derivative), τ_i , was then calculated using a Newton-Raphson iteration method. The convective velocity was obtained from

$$U_c(x_m, y_n) = \frac{1}{4} \sum_{i=-2, -1, 1, 2} \frac{\xi_{x,i}}{\tau_i} \quad (25)$$

The axial coherence length scale L_τ in Eq. 13 is the $1/e$ width of the envelope of the peaks in the space-time correlation exemplified by Fig. 10.

C. Distribution of Convective Velocity

Figure 11 shows contour maps of U_c/U_j on the $x-y$ plane, along with the distributions of mean axial velocity and turbulent kinetic energy. Because this is a subsonic jet, the convective velocity inside the jet flow is subsonic. Note that the computation of U_c in the potential core near the nozzle exit was not reliable because the pressure fluctuations there are very weak. For a given axial location, U_c declines with radial location from the centerline until it reaches a minimum value inside the jet near the edge of the jet. This is consistent with past experimental works that found that U_c “follows” the mean velocity \bar{u} inside the jet. With further increase in the radial location, U_c rises and transitions from subsonic to supersonic. The transition point here is $U_c/U_j = 1.2$ and, as shown in Fig. 11c, it defines a conical-like surface around the jet. Defining the edge of the jet as the boundary between rotational and irrotational flow (a quantitative criterion will follow), the pressure field on the edge contains the full hydrodynamic component which can be thought of as the footprint of the turbulent motion inside the jet. The pressure field on the edge also contains an acoustic (propagating) component, which in this case is weak because the jet is subsonic. Because this is not a very high speed jet, it is reasonable to treat the acoustic field on the edge and outward as linear, and thus apply linear propagation methods. The hydrodynamic field is evanescent and thus decays rapidly with distance, the decay rate being proportional to the local characteristic frequency³⁰ (or inversely proportional the local coherence scale). At some radial distance, only the acoustic component remains. This is the transition point where U_c become sonic. Outside the transition “cone”, the entire pressure field is acoustic.

We discuss the LES statistics on the radiator surface (edge of jet) as defined by Eq. 10 with $\kappa = 0.01$. Figure 12 illustrates the determination of U_c and clarifies the concepts discussed above. Plotted are the radial distributions of velocity gradient magnitude (normalized by the maximum value), \bar{u}/U_j , and U_c/U_j at $x/D_j = 4.0$. The figure allows a more quantitative assessment of the trends discussed in connection with contour maps of Fig. 11. Starting from the jet centerline, U_c initially follows the mean velocity, reaches a minimum, and then starts rising *within* the rotational region of the jet. The edge of the jet, y_{edge} , is defined as the point where $|d\bar{u}/dy|/|d\bar{u}/dy|_{max} = 0.01$. The corresponding $U_c/U_j = 0.57$, which is our selection for the convective speed at this particular x -location. For $y > y_{edge}$, U_c/U_j keeps increasing and the pressure field becomes purely acoustic at $U_c/U_j = 1.2$, which corresponds to $U_c/a_\infty = 1.0$.

D. Azimuthal Correlations

Azimuthal correlations were performed on the rings of Fig. 13. For each axial location, azimuthal correlations were calculated at the radial locations of the lipline (practically identical to the location of peak TKE for $x/D_j \leq 10$), edge of jet as defined in Section II.B, and boundary of the purely acoustic field as described in Fig. 12. The normalized pressure correlation is computed according to

$$R_{pp}(x, y; \Delta\phi) = \frac{\langle p'(x, y, \phi, t) p'(x, y, \phi + \Delta\phi, t) \rangle}{p_{rms}^2(x, y)} \quad (26)$$

which reflects the axial symmetry of the statistics for this round jet. The azimuthal coherence is given by

$$\gamma^2(x, y, \omega; \Delta\phi) = \frac{|S_{12}(x, y, \omega)|^2}{S_{11}(x, y, \omega)S_{22}(x, y, \omega)} \quad (27)$$

where 1 and 2 represent ring locations ϕ and $\phi + \Delta\phi$, and S_{ij} is the cross-spectral density.

Figure 14 plots azimuthal correlations at the three radial locations and for $x/D_j = 2$ and 6. The correlations widen with increasing x , reflecting the larger integral scale of the flow. They also widen with increasing radial distance. At $x/D_j = 2$, the $1/e$ width of the correlation on the lipline is 15° and increases to 35° at the edge and to 75° at the acoustic boundary. At $x/D_j = 6$, near the end of the potential core, the above values roughly double. The increase in azimuthal scale with increasing radial distance from the jet edge is caused by the spreading of the sound emitted by the partial field; it is purely a propagation effect and can be readily calculated using the methods proposed by Refs. 13 and 15. The reasons for the widening of the correlation from the lipline to the edge are not clear but may also involve propagation effects within the jet flow.

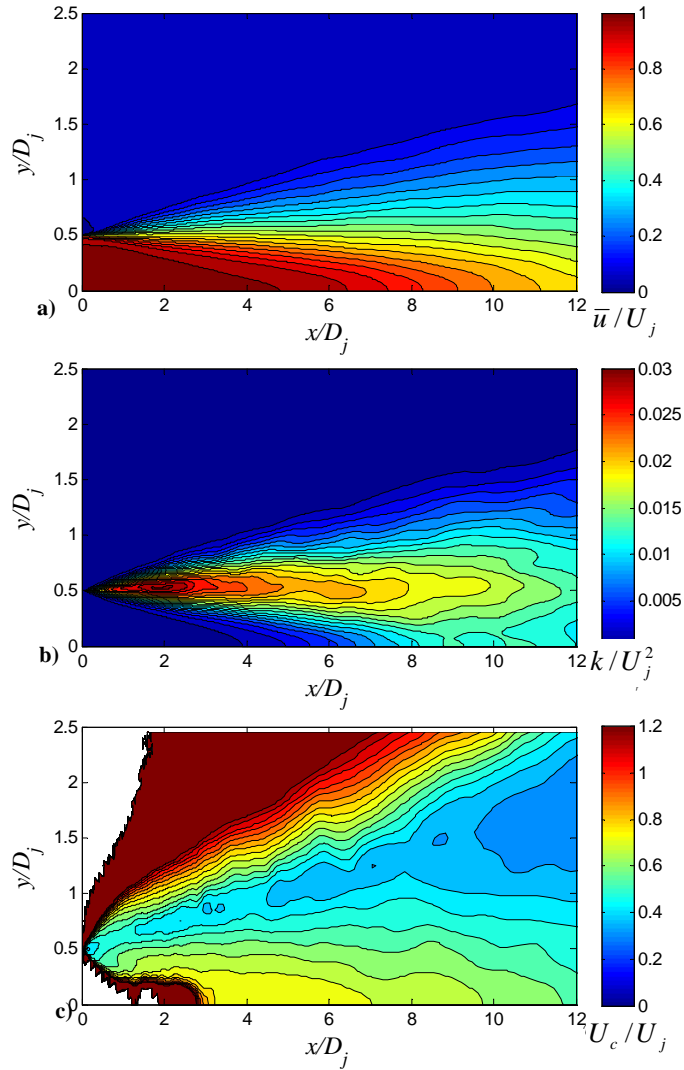


Figure 11. Contour maps on $x - y$ plane of statistics for LES-computed jet: a) mean axial velocity \bar{u}/U_j ; b) turbulent kinetic energy k/U_j^2 ; and c) convective velocity U_c/U_j .

It is instructive to examine the frequency content of the azimuthal correlation by studying the coherence. Figure 15 plots contour maps of the coherence versus $\Delta\phi$ and Strouhal number corresponding to the correlations of Fig. 14. The spreading characteristics discussed above are evident, as is the marked decrease in correlation angle with increasing frequency. Figure 16 plots cross-sections of the coherence map at $x/D_j = 4$, $r/D_j = 1.15$ (edge). The coherence reaches zero at $\Delta\phi = 90^\circ$ for $Sr = 0.2$ and $\Delta\phi = 60^\circ$ for $Sr = 1.0$. This indicates that the partial fields are highly localized in the azimuthal direction.

E. Azimuthal Reconstruction of Partial Field

Assuming the partial field representation of Eq. 1, it is in fact possible to reconstruct the azimuthal shape of the partial field from the azimuthal coherence. Given that the partial field is periodic in ϕ , its pressure distribution at a given frequency can be written as the Fourier series

$$q(\phi - \phi') = \sum_{n=-\infty}^{\infty} C_n e^{in(\phi - \phi')} \quad (28)$$

$$C_n = \frac{1}{2\pi} \int_{-\pi}^{\pi} q(\phi) e^{-in\phi} d\phi$$

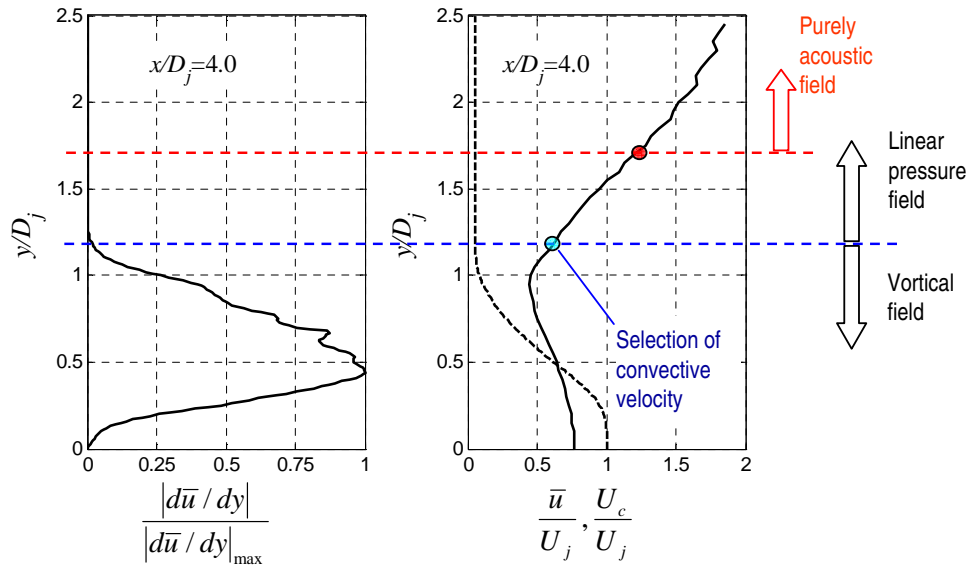


Figure 12. Radial distributions of mean velocity gradient, normalized by maximum value, and convective velocity. Dashed line on right subfigure plots the mean axial velocity. Relevant jet regions are identified.

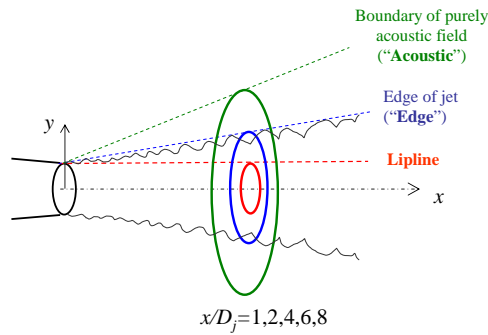


Figure 13. Locations of azimuthal correlations.

Consider the pressures at ϕ_1 and ϕ_2 and form the product

$$q_1 q_2^* = \sum_{n=-\infty}^{\infty} \sum_{m=-\infty}^{\infty} C_n C_m^* e^{i(n\phi_1 - m\phi_2)} e^{i(m-n)\phi'} \quad (29)$$

The azimuthal coherence is $\langle q_1 q_2^* \rangle$, where $\langle \rangle$ now denotes the expectation or ensemble average. Let $f(\phi')$ denote the pdf of ϕ' . The coherence is

$$\langle q_1 q_2^* \rangle = \int_{-\pi}^{\pi} q_1 q_2^* f(\phi') d\phi' \quad (30)$$

For an axisymmetric jet the pdf on the ring (x, r) must be uniformly distributed over $[-\pi, \pi]$, therefore $f(\phi') = 1/(2\pi)$. Inserting Eq. 29 and realizing

$$\int_{-\pi}^{\pi} e^{i(m-n)\phi'} d\phi' = 2\pi \delta_{mn}$$

we obtain

$$\langle q_1 q_2^* \rangle = \sum_{n=-\infty}^{\infty} |C_n|^2 e^{in\Delta\phi} \quad (31)$$

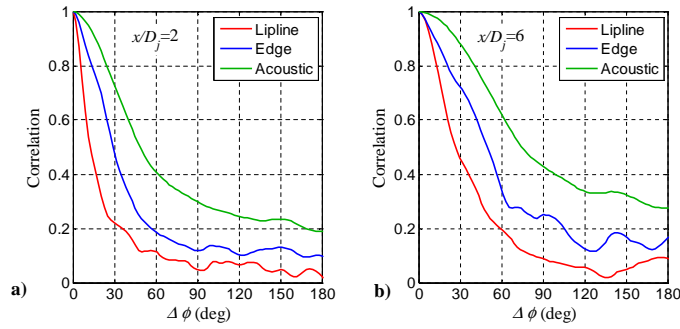


Figure 14. Azimuthal correlations at various radial locations. a) $x/D_j = 2$; b) $x/D_j = 6$.

Knowledge of the azimuthal coherence thus yields the Fourier coefficients $|C_n|^2$. Because the partial field is symmetric with $\Delta\phi$, the coefficients C_n are real and readily calculated as the square root of the corresponding coefficients of the coherence. The partial field is thus reconstructed. Its Fourier coefficients have a wider distribution (versus n) than those of the coherence, which means that the partial field is narrower than the coherence.

Figure 17 reproduces the coherence at $Sr = 0.2$ of Fig. 16 (with some smoothing applied) and overlays the reconstructed partial field. The $1/e$ width of the coherence is 40° while that of the partial field is 20° . So, even at low frequency, events on the radiator surface appear to have very limited azimuthal extent.

V. Comparison of RANS- and LES-Derived Statistics

Having reviewed the statistics and physical insights generated by the RANS and LES solutions, we compare statistical quantities of relevance to the modeling discussed in Sections I and II. The key question is to what extent can the RANS solution provide physically meaningful scales that can guide the construction of the wavepacket partial field. The axial distribution of a given statistical quantity will be evaluated on: the edge of the jet, based on LES-derived correlations (LES-edge); the locus of peak kinetic energy, based on LES-derived correlations (LES- k_{max}); and the the locus of peak kinetic energy, based on RANS-derived scales (RANS- k_{max}). For the RANS-derived correlation length and time scales, the coefficients were determined by the acoustic-analogy based matching of far-field SPL spectra.

Figure 18 plots the axial distribution of the convective velocity U_c . There is good agreement between LES-edge and RANS- k_{max} for $x/D_j \leq 8$, with some divergence downstream. The LES- k_{max} and RANS- k_{max} distributions are very close to each other, which is not surprising given the very similar mean flow fields. Considering that the dominant noise sources for this jet are contained within the first ten or so diameters, the agreement between RANS and LES is deemed promising. Further work is needed to refine the U_c selection criterion for the jet region downstream of the potential core.

The distribution of the axial correlation scale L_τ is plotted in Fig. 19. Here we note that RANS- k_{max} under-predicts LES-edge by about 30% overall, even though the initial “bulge” in the LES trend could be due to the grid not being fine enough. The RANS-based distribution is closer to LES- k_{max} , which is perhaps the more meaningful comparison. The data indicate a widening of the axial correlation with radial distance from the k_{max} location, analogous to the widening of the azimuthal correlation noted in Section IV.D. This trend cannot possibly be predicted by RANS and an empirical correction would need to be applied to the RANS-based correlation (here, a factor of ~ 1.3) to match the distribution on the radiator surface.

The distribution of the azimuthal correlation angle Φ , plotted in Fig. 20, follows similar trends as the axial correlation scale. There is reasonable agreement between LES- k_{max} and RANS- k_{max} , but the RANS- k_{max} distribution under-predicts by at least a factor of 2 the LES-edge distribution. The falling trend of LES-edge for $x/D_j > 4$ is not deemed physical and is probably due to resolution issues with the LES grid. As with the axial correlation, a correction factor would be required to apply the RANS-based scale on the radiator surface.

Finally, we compare the frequency content of the jet as given by LES-edge and RANS- k_{max} . For the LES data, the Strouhal number of the peak of the auto-spectral density was found for each axial location. The

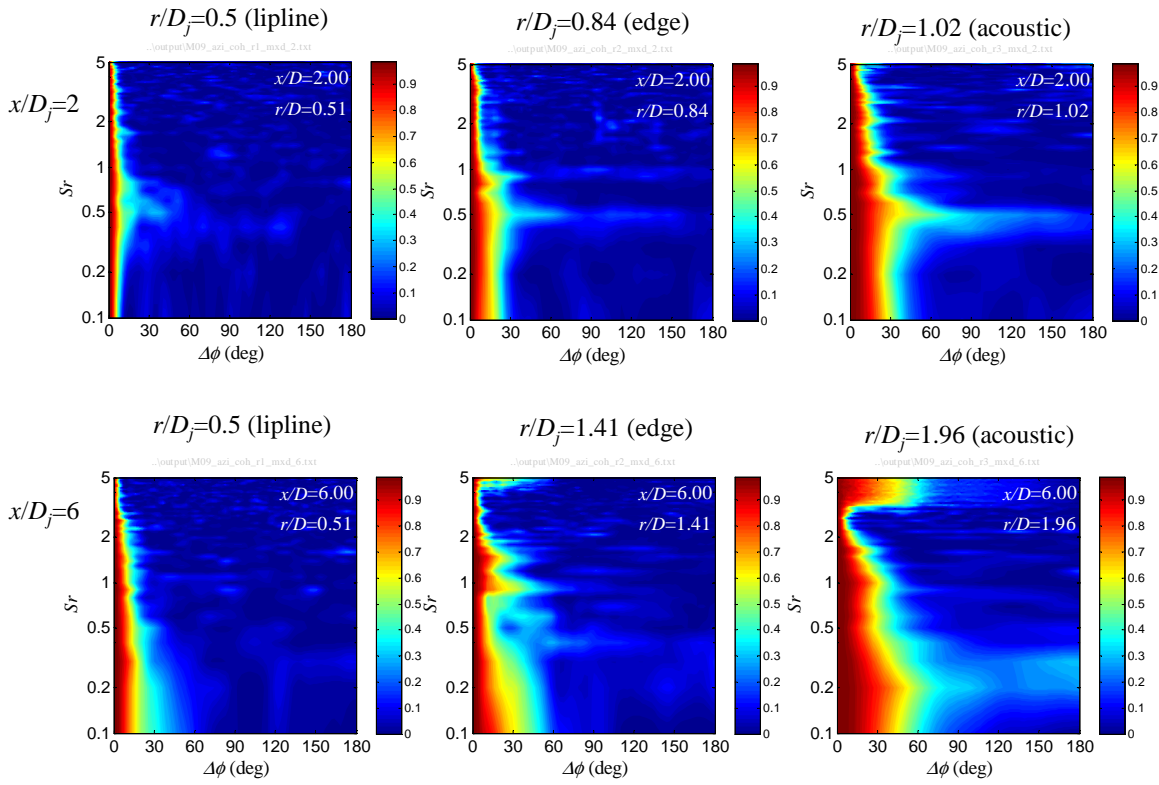


Figure 15. Azimuthal coherence maps.

RANS-based Strouhal number is based on the specific dissipation,

$$Sr = \frac{\Omega D_j}{2\pi U_j}$$

As shown in Fig. 21, the two results are in good agreement. This plot is critical for determining the mean axial location of the partial field for a given frequency, and it appears that RANS can provide fairly accurate guidance in this respect.

VI. Concluding Remarks

The design of new aircraft engines is increasingly influenced by impacts on community noise and personnel exposure in the vicinity of the aircraft. Designers need low-cost predictive tools that can generate reliable solutions in the matter of hours. For jet noise this is an immense challenge that requires the right mix of fundamental physics and empiricism. While there are many ways to formulate equivalent sources for jet noise, the wavepacket model is perhaps the most physically relevant because it captures the fundamental nature of shear layer instabilities in the jet. Its prescription on a near-field surface surrounding the jet, the so-called radiator, hold promise as a low-cost source formulation. Nevertheless, there are complexities associated with the randomness of the source. This is an inherently stochastic model, requiring the synthesis of a number of partial fields, and their propagated sound, to obtain the critical statistics of the pressure field on and off the radiator surface.

The present study is concerned with the modeling of the distribution of correlation scales, frequency distribution, and convective velocity on the radiator surface, defined here as the boundary between the inner rotational field and the outer linear field. These quantities serve as constraints in the parameterization of the source that would lead to determination of the shape of each partial field. The ability of low-cost Reynolds Averaged Navier Stokes (RANS) solution of the flow field to guide the wavepacket formulation is assessed. The RANS solution is accompanied by acoustic analogy based matching of the far-field spectra to determine the coefficients of the appropriate time and length scales. The RANS-derived velocity, length, and time

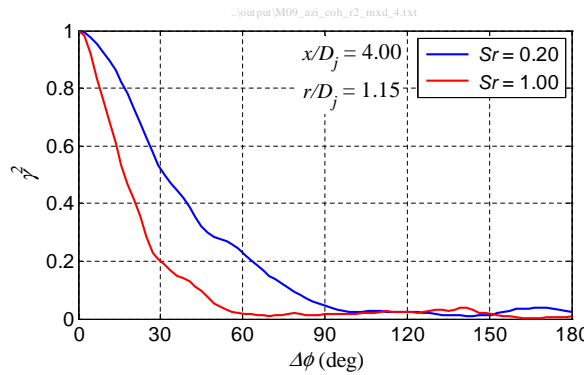


Figure 16. Azimuthal coherence at $x/D_j = 4$, $r/D_j = 1.15$ (edge).

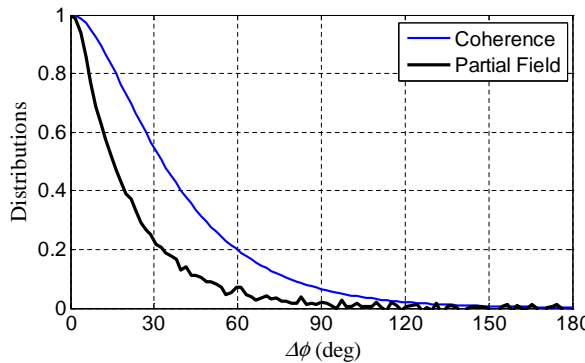


Figure 17. Reconstruction of azimuthal shape of partial field at $Sr = 0.2$.

scales are compared with those obtained using Large Eddy Simulation (LES) of a cold Mach 0.9 jet. The RANS quantities are assessed on the surface peak turbulent kinetic energy (k_{\max}) while the LES statistics are computed on the radiator surface.

The comparisons indicate good agreement on the convective velocity, which is perhaps the most critical quantity in the modeling. There is general agreement between LES and RANS on the correlation scales on the k_{\max} surface; however, the LES indicates that those scales widen from the k_{\max} surface to the radiator surface. Consequently the RANS solution under-predicts the correlation scales on the radiator surface. Correction factors are thus needed to compensate for this difference.

The LES provides additional physical insights into the noise source. The radial distribution of convective velocity U_c , determined by space-time correlations of the pressure, follows the declining radial trend of the mean velocity in the vicinity of the center of the jet. However, near the edge of the jet but still within the rotational flow, U_c starts increasing with radial distance. This reversal suggests that U_c near the edge of the jet is influenced by the footprint of the most energetic eddies in the flow, which occur on or near the k_{\max} surface, rather than disturbances traveling with the local mean velocity.

The LES also sheds light on the azimuthal correlation of the pressure field. The azimuthal correlation angle increases rapidly with radial distance away from the radiator surface, an effect that is purely propagational. Thus, measurement of the azimuthal correlation (or coherence) even at a small distance away from the edge of the jet will provide an over-estimate of the azimuthal scale of the source. Under certain formulations of the wavepacket partial field, the azimuthal shape of the partial field can be reconstructed from the azimuthal coherence. The reconstruction shows a very narrow azimuthal distribution, even at Strouhal numbers as low as 0.2. It is thus suggested that the source is highly uncorrelated in the azimuthal direction.

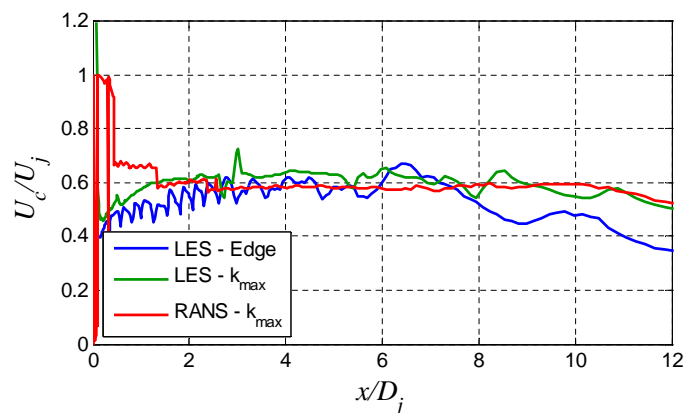


Figure 18. Axial distribution of convective velocity U_c .

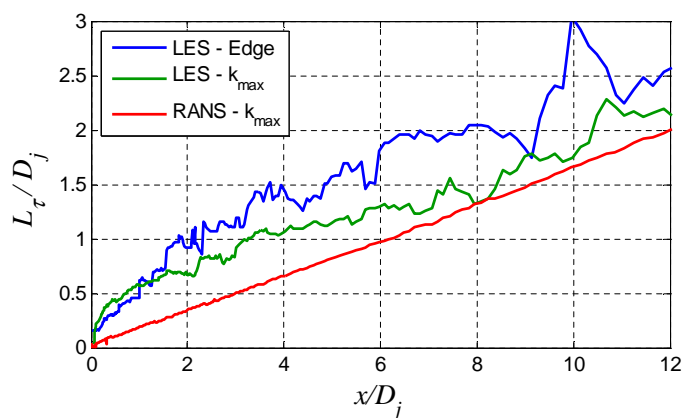


Figure 19. Axial distribution of axial correlation scale L_τ .

References

- ¹Brown, G. and Roshko, A., "On Density Effects and Large Structure in Turbulent Mixing Layers," *Journal of Fluid Mechanics*, Vol. 64, 1974, pp. 775–816.
- ²Ho, C., "Near Field Pressure Fluctuations in a Circular Jet," NASA CR-179847, Nov. 1985.
- ³Zaman, K., "Flow Field and Near and Far Sound Field of a Subsonic Jet," *Journal of Sound and Vibration*, Vol. 106, No. 1, 1986, pp. 1–16.
- ⁴Avital, E. J., Sandham, N. D., and Luo, K. H., "Mach Wave Radiation by Mixing Layers. Part I: Analysis of the Sound Field," *Theoretical and Computational Fluid Dynamics*, Vol. 12, 1998, pp. 73–90.
- ⁵Morris, P., "A Note on Noise Generation by Large Scale Turbulent Structures in Subsonic and Supersonic Jets," *International Journal of Aeroacoustics*, Vol. 8, No. 4, 2009, pp. 301–316.
- ⁶Reba, R., Narayanan, S., and Colonius, T., "Wave-Packet Models for Large-Scale Mixing Noise," *International Journal of Aeroacoustics*, Vol. 9, 2010, pp. 533–558.
- ⁷Jordan, P. and Colonius, T., "Wave Packets and Turbulent Jet Noise," *Annual Review of Fluid Mechanics*, Vol. 45, 2013, pp. 173–195.
- ⁸Baqui, Y. B., Agarwal, A., and Cavalieri, A. V. G., "A Coherence-Matched Linear Model for Subsonic Jet Noise," AIAA 2014-2758, Jun 2014.
- ⁹Fuchs, H., "Space Correlations of the Fluctuating Pressure in Subsonic Turbulent Jets," *Journal of Sound and Vibration*, Vol. 23, No. 1, 1972, pp. 77–99.
- ¹⁰Ukeiley, L. and Ponton, M., "On the Near Field Pressure of a Transonic Axisymmetric Jet," *AIAA Journal*, Vol. 40, 2002, pp. 1735–1744.
- ¹¹Viswanathan, K., Underbrink, J., and Brusniak, L., "Space-Time Correlation Measurements in the Near Field of Jets," *AIAA Journal*, Vol. 49, 2011, pp. 1577–1599.
- ¹²Sreenivasan, K., "The Azimuthal Correlations of Velocity and Temperature Fluctuations in an Axisymmetric Jet," *Physics of Fluids*, Vol. 27, No. 4, 1983, pp. 867–875.
- ¹³Papamoschou, D., "Wavepacket Modeling of the Jet Noise Source," AIAA 2011-2835, June 2011.

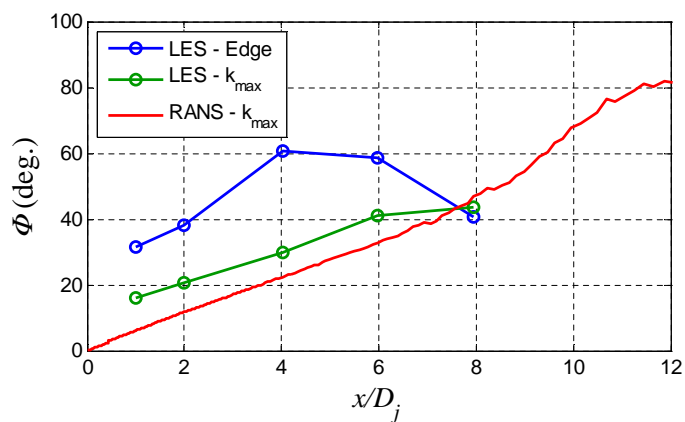


Figure 20. Axial distribution of azimuthal correlation angle Φ .

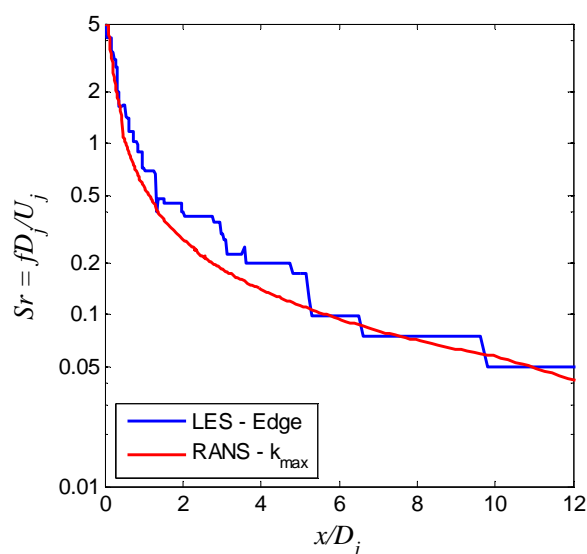


Figure 21. Axial distribution of characteristic Strouhal number.

¹⁴Vold, H., Shah, P., Morris, P., Dongle, Y., and Papamoschou, D., "Axisymmetry and Azimuthal Modes in Jet Noise," AIAA 2012-2214, June 2012.

¹⁵Papamoschou, D. and Rostamimoneji, S., "Modeling of Noise Reduction for Turbulent Jets with Induced Asymmetry," AIAA 2012-2158, June 2012.

¹⁶Papamoschou, D., "Prediction of Jet Noise Shielding," AIAA 2010-0653, Jan. 2010.

¹⁷Papamoschou, D., Xiong, J., and Liu, F., "Reduction of Radiation Efficiency in High-Speed Jets," AIAA 2014-2619, June.

¹⁸Bogey, C., Bailly, C., and Juve, D., "Computation of Flow Noise Using Source Terms in Linearized Euler's Equations," *AIAA Journal*, Vol. 40, No. 2, 2002, pp. 235–243.

¹⁹Xiong, J., Nielsen, P., Liu, F., and Papamoschou, D., "Computation of High-Speed Coaxial Jets with Fan Flow Deflection," *AIAA Journal*, Vol. 48, No. 10, 2010, pp. 2249–2262.

²⁰Jameson, A., Schmidt, W., and Turkel, E., "Numerical Solutions of the Euler Equations by Finite Volume Methods Using Runge-Kutta Time Stepping Schemes," AIAA 1981-1259, January 1981.

²¹Menter, F., "Two-Equation Eddy-Viscosity Turbulence Models for Engineering Applications," *AIAA Journal*, Vol. 32, No. 8, 1994, pp. 1598–1605.

²²Spalart, P. R., Jou, W. H., Strelets, M., and Allmaras, S. R., "Comments on the Feasibility of LES for Wings, and on a Hybrid RANS/LES Approach," 1st AFOSR Int. Conf. on DNS/LES, Ruston, LA, August 1997.

²³Roe, P. L., "Approximate Riemann Solvers, Parameter Vectors and Difference Schemes," *Journal of Computational Physics*, Vol. 46, No. 2, 1980, pp. 357–378.

²⁴Shur, M. L., Spalart, P. R., and Strelets, M. K., “Noise Prediction for Increasingly Complex Jets. Part I: Methods and Tests,” *International Journal of Aeroacoustics*, Vol. 4, No. 3, 2005, pp. 213–246.

²⁵Spalart, P. R. and Allmaras, S. R., “A One-Equation Turbulence Model for Aerodynamic Flows,” AIAA 1992-0439, January 1992.

²⁶Morris, P. J. and Farassat, F., “Acoustic Analogy and Alternative Theories for Jet Noise Prediction,” *AIAA Journal*, Vol. 40, No. 4, 2002, pp. 671–680.

²⁷Shanno, D. F. and Phua, K. H., “Minimization of Unconstrained Multivariate Functions,” *ACM Transactions on Mathematical Software*, Vol. 6, No. 4, 1976, pp. 618–622.

²⁸Karabasov, S., Afsar, M., Hynes, T., Dowling, A., McMullan, W., Pokora, C., Page, G., and Guirk, J., “Jet Noise: Acoustic Analogy Informed by Large Eddy Simulation,” *AIAA Journal*, Vol. 48, No. 7, 2010, pp. 1312–1325.

²⁹Lau, J., Morris, P., and Fisher, M., “Measurements in Subsonic and Supersonic Free Jets Using a Laser Velocimeter,” *Journal of Fluid Mechanics*, Vol. 93, No. 1, 1979, pp. 1–27.

³⁰Guitton, A., Jordan, P., and Laurendau, E., “Velocity Dependence of the Near Pressure Field of Subsonic Jets: Understanding the Associated Source Mechanisms,” AIAA 2007-3661, June 2007.